Materials Today Catalysis 11 (2025) 100129

Contents lists available at ScienceDirect

Materials Today Catalysis

journal homepage: www.journals.elsevier.com/materials-today-catalysis

Impact of zeolite properties on catalytic hydrodeoxygenation: Spatially segregated metal-acid site engineering for enhanced cascade efficiency

Shengzhe Ding [a,b], Min Hu [b], Ushna Khalid [b], Run Zou [b], Carmine D'Agostino [b,c], Yani Peng [b], Qiang Zhang [d], Yilai Jiao [e], Christopher M.A. Parlett [b,f,g,*], Xiaolei Fan [b,h,*]

[a] Institute of Catalysis Science, Beijing Research Institute of Chemical Industry, Sinopec, Beijing 100013, China
[b] Department of Chemical Engineering, The University of Manchester, Manchester M13 9PL, UK
[c] Dipartimento di Ingegneria Civile, Chimica, Università di Bologna, Bologna 40131, Italy
[d] State Key Laboratory of Heavy Oil Processing, China University of Petroleum, Qingdao 266580, China
[e] Shenyang National Laboratory for Materials Science, Chinese Academy of Sciences, Shenyang 110016, China
[f] University of Manchester at Harwell, Harwell Science and Innovation Campus, Didcot, Oxfordshire OX11 0DE, UK
[g] UK Catalysis Hub, Rutherford Appleton Laboratory, Harwell, Oxfordshire, OX11 0FA, UK
[h] Nottingham Ningbo China Beacons of Excellence Research and Innovation Institute, Ningbo 315100, China

ARTICLE INFO

Keywords:
Hydrodeoxygenation (HDO)
Zeolites
Pd nanoparticles
Spatial separation
Biofuel
Cascade catalysis

ABSTRACT

To reduce the environmental impact of hydrodeoxygenation (HDO) while enhancing process economics, it is crucial to develop advanced catalytic materials that enable HDO under milder conditions, suppress decarboxylation/decarbonylation (DCOx), and eliminate auxiliaries, all while maximising target product yield. Spatial segregation of metal and acid sites has emerged as an effective strategy for improving HDO efficiency in fatty acid conversion. This study explores the influence of zeolitic carrier porosity and acidity on HDO, employing Pd nanoparticles as the metal catalyst and lauric acid as the model substrate. The findings reveal that acidity and mesoporosity are key determinants of substrate conversion, product selectivity, and overall catalytic performance within the same zeolitic framework (MFI ZSM-5). High acidity and hydrophilicity in ZSM-5 zeolites hinder lauric acid conversion by retaining water within the framework, which would adversely affect reaction equilibria in the HDO cascade, whereas mesoporosity in hierarchical ZSM-5, which enhances mass transport, is beneficial for conversion and dodecane formation. For hierarchical ZSM-5, produced via desilication, the less acidic PdNP/HMZSM5-DA25 (25 reflecting the original Si:Al ratio) yields 2.5 times more dodecane than more acidic but less mesoporous PdNP/HMZSM5-DA15 (Si:Al of 15). Expanding this investigation to different zeolitic frameworks (Pd nanoparticles supported on USY, BETA, and ZSM-5) demonstrates that larger micropores further facilitate diffusion and improve catalytic efficiency. PdNP/HUSY-DA exhibits a 32% improvement over PdNP/HMZSM5-DA25, with a dodecane production rate of 6.1 $mmol_{dodecane}\ g_{catalyst}^{-1}\ h^{-1}$, ranking it among the most superior state-of-the-art HDO systems at comparable conditions. This study validates the spatial segregation of active sites as a robust strategy for stabilising Pd nanoparticles and improving catalyst durability in cascade HDO processes. Fine-tuning zeolite properties is essential for optimising catalyst design to achieve efficient and sustainable biofuel production via HDO.

1. Introduction

Biofuels derived from sustainable non-edible biomass represent a key player in advancing the circular economy and achieving net zero within the chemical industry [1]. A plethora of chemical pathways from biomass to biofuels are known, with hydrodeoxygenation (HDO) representing one potential option. The employment of this approach for fatty acid conversion to C_8–C_{16} alkanes provides an interesting and feasible route to sustainable aviation fuel (SAF) and, thus, a pathway to the decarbonisation of the aviation sector [2,3]. However, several issues persist within current catalytic HDO processes, with those that are of specific concern to fatty acid upgrading, including undesirable side reactions, a requirement of co-feeding H_2S (or dimethyl disulphide), high reaction temperature (>340 °C), and erosion [2]. These diminish the

* Corresponding authors at: Department of Chemical Engineering, The University of Manchester, Manchester M13 9PL, UK.
E-mail addresses: christopher.parlett@manchester.ac.uk (C.M.A. Parlett), xiaolei.fan@manchester.ac.uk (X. Fan).

https://doi.org/10.1016/j.mtcata.2025.100129
Received 18 August 2025; Received in revised form 26 September 2025; Accepted 14 November 2025
Available online 15 November 2025

credentials of fatty acid HDO and contribute to poor overall economics relative to petroleum-derived jet fuel [4–6]. Side reactions, namely decarboxylation or decarbonylation (DCO_x) of the acid and aldehyde (product of partial reduction), release CO_2 and CO, the latter a common catalyst poison. Whilst the latter is not overly a concern for conventional HDO catalysts, which are comprised of transition metal sulphides, co-feeding H_2S is required to maintain the active species; however, this simultaneously leads to sulfur emission [7]. Moreover, this class of active species is deployed in conjunction with high processing temperatures.

Conventional noble metal catalysts (e.g., Pd/C) can produce alkanes from the conversion of fatty acids, including at relatively mild temperatures < 300 °C, but this proceeds predominantly via the DCO_x pathways, for which CO becomes problematic [2]. Introducing acidic sites to the system increases the propensity for HDO, with synergy between the two sites key. The benefit arises for either a catalytic system comprising two monofunctionalised catalysts as a physical mixture or where two sites are present as a random combination on a single material, i.e., a bifunctional material. Thus, this symbiosis can occur over a range of length scales, from the picometer, where sites are adjacent in a single architecture, to the micrometre, for physical mixtures. Therefore, it is the studious combination of these two species which is critical in driving the HDO process, which can be considered a cascade process. After the initial hydrogenation of a fatty acid to a fatty alcohol, dehydration yields an alkene intermediate, which is finally hydrogenated to the desired alkane. This mechanism retains the hydrocarbon chain length of the initial substrate, producing water as the byproduct. Within the three-step cascade, metallic sites facilitate the first and last steps, while acidic sites are active for the middle step [8].

Zeolites are ubiquitous within the field of solid acid catalysis, with the inherent Brønsted acidity of the aluminosilicates framework utilised industrially for reactions including catalytic cracking, isomerisation, and aromatisation [9,10]. Applying such species when designing HDO catalysts is therefore intuitive, as demonstrated by their use to support Pd, Pt and Ni [2,11–13]. While enabling milder reaction conditions (<250 °C), HDO selectivity is compromised to a degree by DCO_x, with HDO:DCO_x often less than 2. Increasing metal dispersion can exacerbate this unwanted trend, with highly dispersed Pd supported on hierarchical H-ZSM-5 possessing an equal tendency for HDO and DCO_x [14]. Increased dispersion coupled with random uncontrolled deposition on the support should elevate the interaction between the metal and acid sites, which in turn can increase DCOx [14–16]. In contrast, spatially segregating the metal and acid sites through the use of a physical mixture of two catalysts (ZSM-5 and Pd/CuZnAl) can increase the HDO pathway, with both catalysts vital if the alkane is to be produced [17]. However, such spatial separation here is at least in the microns, and possibly much more; thus, efficient diffusion between these two sites is far from optimal. Fine-tuning the spatial distance between the metal and acid sites is thus likely critical in regulating the HDO performance. Routes to achieve control of active site separation have utilised differences in chemical properties, including those between the support and binder material used in commercial catalyst preparation [18] or through tailoring of surface chemistry of different pore regions in hierarchical bimodal porous architectures [19]. The latter has also been realised through the development of bespoke synthesis strategies [19,20], including for HDO via spatial compartmentalisation of acid and platinum group metals in distinct individual regions [21]. Specifically, Pd nanoparticles (NPs) with diameter of ~5 nm are controllably deposited within the mesopores (and externals surfaces) of hierarchical ZSM-5 in which the inherent Brønsted acid sites of the support are preserved only within the micropores, i.e., using size limitations to spatial segregation Pd and acid site at the nanoscale, resulting in a possible minimal distance between these of the distance from one mesopore to an adjoining micropore. Such a configuration is highly beneficial to facilitating the HDO cascade (outline above), with an HDO:DCO_x ratio of ~5. The unique configuration within the catalyst allows each step to occur individually over the corresponding site, while diffusion within and between the two different pores dictates the order in which different catalytic species are encountered. Moreover, the simplicity of the synthetic strategy makes it prime for further investigation and development.

Building on the initial success in the rational design and synthesis of an HDO catalyst targeted for the three-step cascade, i.e., the spatial compartmentalising of two sites for HDO within individual pore networks of hierarchical mesopores-microporous ZSM-5, we report a systematic investigation to expand the approach. Specifically, evaluating the impact of (i) the silicon-to-aluminium ratio (SAR) of the hierarchical zeolites (which is closely linked to Brønsted acidity) for a common parent framework (ZSM-5) and (ii) the zeolite framework type (FAU, BEA and MFI) with a common SAR. For (i), post-synthetic desilication of ZSM-5 with different SAR values (of 40, 15 and 12.5), will evaluate the role of acid site density, whilst the nuance of zeolite framework, including variation in micropore size ~0.74 nm for FAU USY zeolite, ~0.67 nm for BEA beta zeolite and ~0.54 nm for MFI ZSM-5 zeolite, will be gauged via (ii). The HDO of lauric acid is used to scrutinise the impact of tuning these properties.

2. Methods

2.1. Materials and chemicals

ZSM-5 (SAR = 40, NH_3 form), USY (SAR = 15, H form), and Beta (SAR = 12.5, NH_3 form) zeolites were purchased from Zeolyst International. ZSM-5 (SAR = 25, NH_3 form) and ZSM-5 (SAR = 15, NH_3 form) were purchased from Fisher Scientific. Sodium hydroxide (ACROS Organics, ≥99 %), ammonium nitrate (ACROS Organics, ≥98 %), diethylenetriaminepentaacetic acid (DPTA, Sigma Aldrich, ≥99 %), ethylene glycol (EG, Fisher Scientific, ≥99 %), poly(vinyl pyrrolidone) (PVP, Sigma Aldrich, M_w = ~55000), sodium tetrachloropalladate(II) (Sigma Aldrich, ≥98 %), hexane (Sigma Aldrich, ≥95 %), nonane (Sigma Aldrich, ≥99 %), lauric acid (Sigma Aldrich, ≥98 %), and lauryl alcohol (Sigma Aldrich, ≥98 %) were all used as received.

2.2. Preparation of hierarchical zeolites

Zeolites supplied in the NH_3 form were calcinated for 5 h at 550 °C (ramp rate 5 °C min^{-1}) to produce the H-form counterparts (denoted HZSM5-*x*), where *x* is the SAR value of the corresponding parent ZSM-5 zeolite. The protonated forms of the zeolite frameworks were treated by alkaline desilication using the method reported previously [22]. Taking ZSM-5 as an example, HZSM5-*x* (6 g) was vigorously stirred in aqueous NaOH solution (0.2 M, 180 cm^3) at 65 °C for 0.5 h, the solid was isolated by centrifugation (3000 G, 10 min) and washed repeatedly with deionised water to pH neutral. The solid was Na ion-exchanged using aqueous NH_4NO_3 (0.1 M, 180 cm^3) at 80 °C for 3 h in triplicate, with the solid isolated by centrifugation. The solid was dried at 100 °C for 6 h and then calcined in air for 5 h at 550 °C (ramp rate 5 °C min^{-1}) to produce the H-form hierarchical ZSM-5 (denoted HMZSM5-*x*).

Surface Brønsted acidity within mesopores and on the external surface of HMZSM5-*x* was removed by microwave-assisted chelation method [23]. HMZSM5-*x* (1 g) was dispersed in aqueous DPTA (0.16 M, 15 cm^3) under stirring at room temperature (~20 °C). The solution was heated under microwave irradiation (Anton Paar Monowave 400 microwave) to 100 °C (ramp rate 25 °C min^{-1}) and treated isothermally for 15 min. The solid was isolated by centrifugation (3000 G, 10 min) and washed, dried and then calcined for 5 h at 550 °C (ramp rate 5 °C min^{-1}) to produce the H-form hierarchical ZSM-5 in which acidity was only present within the micropores (denoted HMZSM5-DA*x*). For USY and Beta zeolites, the dealumination of the calcined parent support was conducted using the same protocol to produce HUSY-DA and HBETA-DA, respectively.

2.3. Pd NP synthesis

Pd NPs of 4.6 ± 1.3 nm were prepared using a procedure reported by Wang et al [24]. PVP (450 mg) was dissolved in EG (20 cm^3) at 160 °C. A second solution containing Na_2PdCl_4 (155 mg) dissolved in EG (10 cm^3) at 60 °C was added to the PVP-EG solution at 160 °C under stirring at 600 rpm. After 3 h, acetone (60 cm^3) was charged into the solution to precipitate Pd NPs. The solid was isolated by centrifugation (10500 G, 20 min) and washed in triplicate with a water and acetone mixture (1:3, vol/vol). The solid was then dispersed in water (30 cm^3) to form a colloidal solution for further use.

2.4. Spatially segregated catalyst - Pd NP in mesopore and acid sites in micropores

Deposition of Pd NPs on HMZSM5-DA*x* was conducted by wet impregnation. Pd NP colloid (6 cm^3) was mixed with HMZM5-DA*x* (1 g) to yield a catalyst with a nominal 0.4 wt% Pd loading. The slurry was stirred at 20 °C for 18 h and then heated to 50 °C for solvent evaporation. The dried solid was calcined for 2 h at 400 °C (ramp rate 1 °C min^{-1}) and reduced for 2 h at 200 °C under a pure H_2 flow (ramp rate 5 °C min^{-1}, flow rate 100 cm^3 min^{-1}) to yield the catalyst denoted as PdNP/HMZSM5-DA*x*. The same methodology was used to prepare the corresponding metal supported catalysts based on HUSY-DA and HBETA-DA, which were denoted as PdNP/HUSY-DA and PdNP/HBETA-DA, respectively.

2.5. Characterisation of materials

Actual metal loadings were determined by inductively coupled plasma optical emission spectrometry (ICP-OES), preceded by microwave digestion at 220 °C for 15 min in aqua regia. Catalyst loadings were determined to be 0.4 ±0.02 wt%. The SAR of zeolites were measured by X-ray fluorescence (XRF) using a PANalytical MiniPal4 spectrometer at 30 kV and 1 mA.

Powder X-ray diffraction (XRD) was conducted on a Philips X'Pert-PRO theta-theta PW3050/60 diffractometer with a PW3064 sample spinner and X'Celerator 1-D detector (2.122° active length) in Bragg-Brentano geometry using a copper line focused X-ray tube with Ni K_β absorber (0.02 mm; K_β = 1.392250 Å) K_α radiation ($K_{\alpha1}$ = 1.540598 Å, $K_{\alpha2}$ = 1.544426 Å, K_α ratio 0.5, $K_{\alpha ave}$ = 1.541874 Å). Diffraction patterns were collected from 5 to 75 ° 2 theta at 0.0334 ° step and 1.7 s $step^{-1}$.

Nitrogen (N_2) adsorption/desorption isotherms were measured on a Micromeritics ASAP 2020 porosimeter. The materials were degassed under vacuum at 350 °C for 12 h before N_2 physisorption at the liquid nitrogen temperature of −196 °C. The Brunauer–Emmett–Teller (BET) surface area (S_{BET}) was calculated over the relative pressure range of 0.03–0.30, the specific microporous area (S_{micro}) and microporous volume (V_{micro}) were calculated over the relative pressure range of 0.3–0.5 using the *t*-plot method. Pore size distribution was estimated by the Barrett–Joyner–Halenda (BJH) method with Fass correction using the adsorption branch of the isotherms [25].

Ammonia temperature-programmed desorption (NH_3-TPD) was conducted using a Quantachrome ChemBET 3000 system. Catalysts (~50 mg) were pre-treated at 550 °C (ramp rate 5 °C min^{-1}) for 1 h under He (60 cm^3 min^{-1}) and then cooled to 100 °C. A gas mixture of NH_3/He (1:9 vol/vol, 30 cm^3 min^{-1}) was introduced to saturate the catalyst surface (1.5 h), followed by He purge (60 cm^3 min^{-1}) at 100 °C for 2 h to remove physiosorbed NH_3. NH_3-TPD was performed by heating the catalyst from 100 to 600 °C (ramp rate 10 °C min^{-1}) under He (30 cm^3 min^{-1}), with desorbed NH_3 monitored by a thermal conductivity detector (TCD), which was calibrated against a known volume of gas prior to measurements.

High-angle annular dark-field scanning transmission electron microscopy (HAADF-STEM) images were recorded on an FEI Talos F200A equipped with a Schottky field-emission gun and an FEI Super-X 4-detector EDX system. The instrument was operated at an accelerating voltage of 200 kV and an extraction voltage of 4.5 kV with a monochromated energy spread of ~0.25 eV. The HAADF-STEM samples were prepared by dispersing the catalyst in ethanol by ultrasonication for 15 min, followed by drop casting onto 300 mesh copper grids with holey carbon films.

Nuclear magnetic resonance (NMR) relaxation measurements were carried out in a Magritek SpinSolve benchtop NMR spectrometer operating at a ^1H frequency of 43 MHz. T_1 relaxation experiments were performed using an inversion recovery pulse sequence, acquiring 16 experimental points for each experiment with time delay values between 1ms and 1000ms, 16–64 scans and a repetition time of 1000ms [26]. T_2 relaxation experiments were performed with the CPMG (Carr Purcell Meiboom Gill) pulse sequence, with an echo time of 250μs, using 16steps with a number of echoes per step varying in the range 30–70, 64–128 scans and a repetition time of 1000ms [27]. The NMR samples were prepared by soaking the catalyst particles in water or *n*-octane for 48 h, which were then removed from the liquid and placed on a pre-soaked filter paper to remove any excess external liquid. Finally, the catalysts were placed into 5 mm NMR glass tubes, and the experiments were conducted at 20 ± 0.5 °C and atmospheric pressure.

Diffuse reflectance infrared Fourier transform spectroscopy (DRIFTS) of the catalysts was performed on a Bruker Vertex 70 FTIR spectrometer. Samples were treated at 300 ℃ (10 °C min^{-1}) in argon flow (60 cm^3 min^{-1}), with spectra collected at the same temperature. KBr was used for the background. Spectra are an average of 128 scans with a wavenumber resolution of 4 cm^{-1}. Pyridine adsorption at the acid sites was evaluated by Fourier transform infrared (FTIR) spectroscopy, conducted on a Bruker Tensor-27 FTIR spectrometer. The ground sample (sieved to ≥ 300 mesh) was dried at 140 °C for 12 h prior to pyridine (15 cm^3 pyridine) vapour exposure in a vacuum desiccator at −0.1 MPa for 12 h. Following adsorption, the liquid pyridine was removed from the desiccator, and the sample was maintained at −0.1 MPa for 30 min. The sample was dried at 140 °C for 12 h to remove any physiosorbed pyridine. The sample was pressed into a mould to provide a smooth surface for analysis. A spectrum of the zeolite without adsorbed pyridine was used as the background.

2.6. Catalytic HDO of lauric acid to dodecane

Catalyst (0.1 g) was charged into a Parr 4598 autoclave reactor (100 cm^3) with hexane (20 cm^3). The system was purged 5 times with N_2 (5 bar) prior to catalyst reduction for 2 h at 200 °C under H_2 (30 bar) with agitation (1000 rpm). After activation, the reactor was purged with N_2, followed by the addition of lauric acid (0.6 g) dissolved in hexane (20 cm^3) containing nonane (0.1 cm^3) as an internal standard. The system was then pressurised with H_2 (30 bar) and heated to 200 °C. The HDO reaction was initiated by commencing stirring (1000 rpm), with aliquots (~1 cm^3) extracted periodically for reaction profiling, with analysis by off-line gas chromatography on a Perkin Elmer Clarus 500 gas chromatography (GC) with a DB-Wax column (30 m × 25 mm × 0.25 μm). The GC was multipoint calibrated with respect to lauric acid, lauryl alcohol, dodecane and undecane. The quantity of lauryl laurate was estimated based on the method reported by Liaw and Tso [28]. Lauryl alcohol dehydration was conducted under identical conditions but with the omission of the H_2 reduction using lauryl alcohol (0.56 g), hexane (20 cm^3) and nonane (0.1 cm^3).

3. Results and discussion

3.1. Characterisation of ZSM-5 zeolite-based catalysts

The application of a brief alkaline and acid post-synthetic treatment as a route for imparting mesoporosity and, thus, the production of hierarchical ZSM-5 zeolites, imparts no significant detrimental impact on

the zeolite crystalline structure, as identified in Figures S1 and **1a**. XRD reveals comparative characteristic diffraction peaks at 2θ = 7.97°, 8.83°, 23.17°, 24.09°, and 24.48° (representing the (011), (200), (501), (033), and (133) facets of the MFI framework, JCPDS no. 44–0696 [29]). However, the treatment does induce the formation of mesopores within the zeolite framework, as confirmed by N_2 adsorption-desorption isotherms and corresponding BJH pore size distributions (**Figures 1b** and **S2)**. The former clearly reveals a transition in isotherm shape from a type I (parent) [30] to a type IV (hierarchical zeolite), with the more prominent hysteresis indicative of a material possessing greater mesoporosity. Quantification, as shown in Table S1, further confirms this, with the resultant degree of additional mesoporosity proportional to the amount of silicon present in the parent, i.e., ZSM5–40 sees a 316 % increase in mesopore volume after desilication; conversely, the increase drops to only ~123 % for ZSM5–15. For alkaline ZSM-5 desilication, an optimal SAR of 25–50 has been reported (for mesopore formation), as at lower SAR (<20), the increased concentration of tetrahedral framework Al hinders efficient Si extraction [31,32]. Unsurprisingly, the subsequent dealumination treatment with DPTA, which possesses a molecular diameter of 0.9 nm to ensure no extraction from within the micropores, imparts less of a dramatic increase in mesoporosity. Reflecting the lower overall Al content relative to Si; however, likewise, the degree of the impact of the treatment is proportional to the level of the element being targeted for extraction (i.e., an increase in mesopore volume of 28 % vs 9.5 % for SAR of 15 and 40, respectively) [31]. The minimal impact of the dealumination was further apparent from a control study subjecting HZSM5–25, with a middle Al content, to microwave-assisted chelation only (denoted HZSM5-DA25) [23]. The omission of the desilication step results in a negligible increase in mesoporosity (Table S1). The mesopore distributions for all three HMZSM5-DA*x* zeolites are broad, with Figure S2b illustrating that sizes range from ~2–32 nm in diameter, i.e., there is a lack of uniformity in the secondary pores. Moreover, the SAR from XRF reveals that materials after both treatments possess values close to their parent, with values of 36, 26, and 17 for HMZSM5-DA40, HMZSM5-DA25, and HMZSM5-DA15, respectively.

Hydroxyl groups associated with framework Al, extra-framework Al, and isolated silanols [33] present within the HMZSM5-DA*x* zeolites are identified by DRIFTS (Figure S3a). Consistent with expectations, increasing Al content gives rise to a greater presence of extra framework Al (Lewis sites) and an increase in framework Al (Brønsted sites) relative to silanol groups, viz reduced relative contribution from isolated silanol. NH_3-TPD was employed further to probe the acidic properties of the HMZSM5-DA*x* zeolites, as shown in Fig. 1**c,** with quantification reported in Table S2. Fig. 1**c** reveals typical bimodal NH_3 desorption profiles, common for ZSM-5 zeolites, with desorption > 400 °C representing strong acidity from framework Al Si bridging hydroxyls (likely Brønsted acidity), whilst the peak at < 300 °C corresponds to acidity resulting from extra-framework Al and silanols [32,34]. Consistent with DRIFTS, HMZSM5-DA15 shows the highest total acidity at ~10.3 mmol g^{-1} vs 7.7 mmol g^{-1} (HMZSM5-DA25) and 5.4 mmol g^{-1} (HMZSM5-DA40). The higher Al concentration comprises a greater degree of strong Al-$O^{(H)}$-Si, i.e., more Brønsted acid sites (~4.5 mmol g^{-1} from pyridine adsorption) and a greater degree of weaker sites. Consequently, there is a trade-off between mesoporosity and acidity when deploying the post-synthetic treatment, as shown in Fig. 1**d**. However, based on our preliminary study [21], the HDO cascade that these systems are designed for requires both mesoporosity and acidity. Which has a greater influence on overall performance is currently unclear and will be

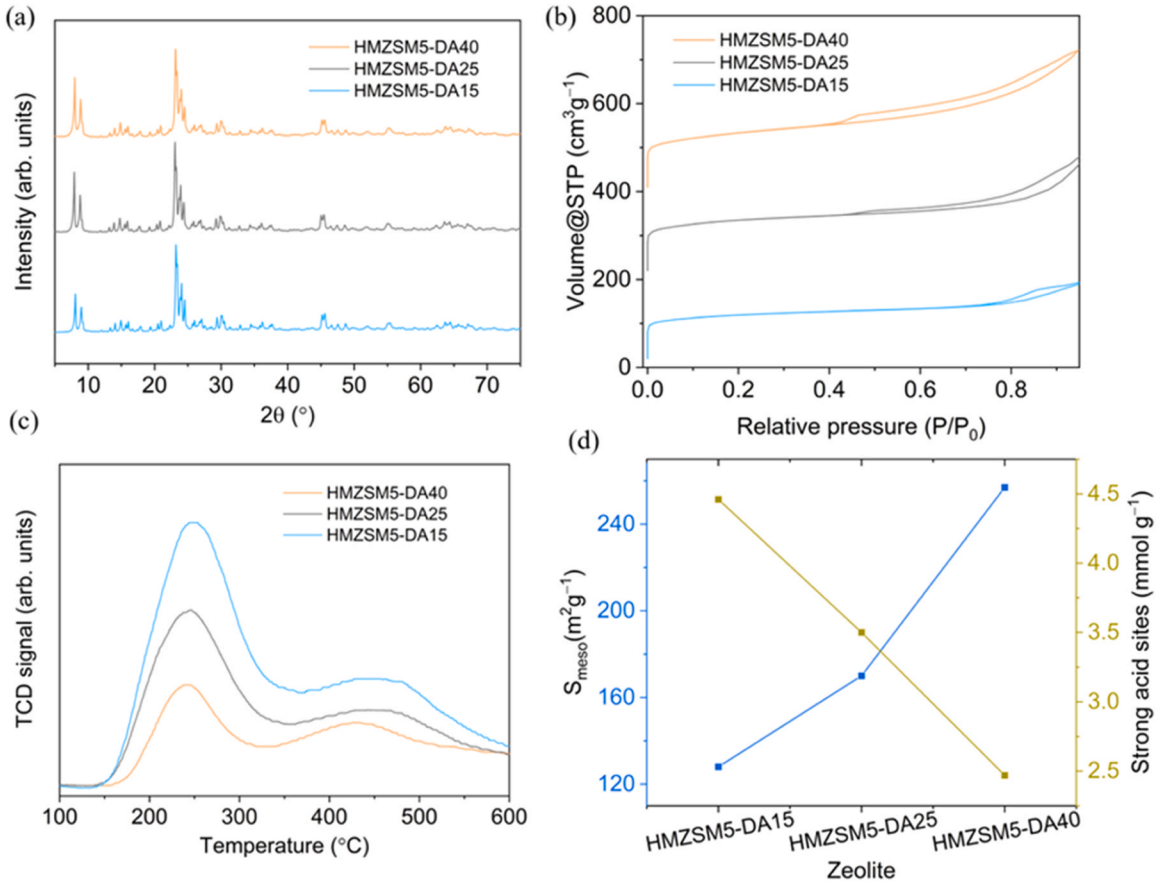

Fig. 1. Physicochemical properties of the HMZSM5-DA*x* zeolites; (a) XRD diffraction patterns; (b) N_2 adsorption-desorption isotherms, to aid visualisation, HMZSM5-DA25 and HMZSM5-DA40 are offset by 250 and 450 cm^3 g^{-1}, respectively; (c) NH_3-TPD profiles; and (d) comparison of mesoporosity and acidity as a function of SAR.

discussed later in detail (in the catalysis section). Further evaluation of the acid sites, via pyridine adsorption (Figure S3b), reveals co-existence of Brønsted and Lewis acid sites, with the ratio of the two comparable for the two lower SAR (10.7 vs 9.3 for HMZSM5-DA15 and HMZSM5-DA25, respectively). However, increasing SAR further significantly increase this ratio to 15, i.e., decreasing Al increases relative Brønsted acidity.

One impact of removing acidity from the mesopores (and external surfaces) via Al extraction by microwave-assisted chelation is an increase in hydrophobicity. This positively impacts catalytic HDO performance either directly, via repulsion of the water byproduct produced during fatty acid reduction and alcohol dehydration, or indirectly, by eliminating unfavourable electronic interactions between acid and platinum group metal sites [21]. To assess the impact of SAR on hydrophobicity, NMR relaxation measurements were performed using water and *n*-octane as probe molecules. Table S3 shows the calculated T_1 and T_2 values for longitudinal and transverse spin relaxation times

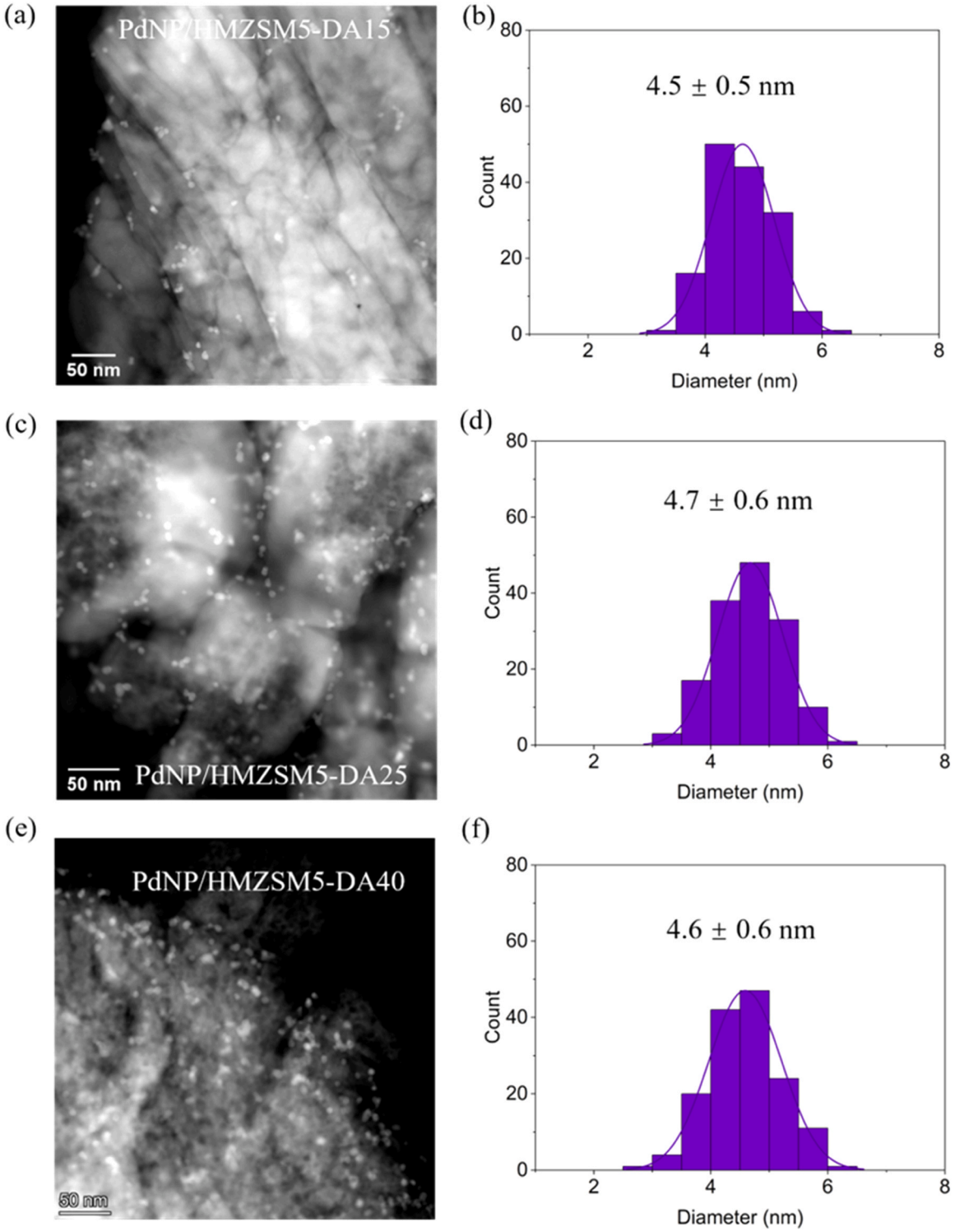

Fig. 2. Representative HAADF-STEM image of (a) PdNP/HMZSM5-DA40, (b) PdNP/HMZSM5-DA25, and (c) PdNP/HMZSM5-DA15; (b), (d) and (f): the corresponding Pd particle size distributions.

resulting from the interaction between probe and HMZSM5-DA zeolites. The affinity of the zeolite towards each probe is reflected in the T_1/T_2 ratio (an increase in ratio usually indicates higher surface affinity) [35], which, when comparing a common framework, are independent of particle morphology and surface/volume ratio [36–38]. Consistent with previous studies [35], we also observed a decreasing trend of T_1/T_2 for water within our ZSM-5 based materials as SAR increases, i.e., HMZSM5-DA15 (highest T_1/T_2) is the more hydrophilic and HMZSM5-DA40 (lowest T_1/T_2) is the more hydrophobic. This switching in affinity is further confirmed by the inverse relation when evaluating T_1/T_2 for *n*-octane, i.e., assessing the oleophilic nature of a material, with HMZSM5-DA40 showing the highest T_1/T_2 for *n*-octane and HMZSM5-DA15 the lowest.

Having fine-tuned the acidity, both in relation to location (micropores only) and density through SAR, of the H-MZSM5-DA*x* zeolites, the next point to address is the complementary platinum group metals sites that are critical to facilitating the first and third steps of the HDO cascade pathway. Preformed Pd NPs of ~5 nm were deposited onto the H-MZSM5-DA*x* zeolites via impregnation. The use of preformed NPs over conventional wet impregnation of a salt is critical to ensuring Pd cannot reside within the micropores of the zeolite framework. HAADF-STEM images of the PdNP/HMZSM5-DA*x* catalysts are shown in Fig. 2. Mesoporosity is clearly apparent in PdNP/HMZSM5-DA40 (Fig. 2**e**), whereas it is less evident in PdNP/HMZSM5-DA15 (Fig. 2**a**), which is consistent with N_2 porosimetry (Table S1). In addition, Pd particle size distributions for each catalyst (Figs. 2**b**, 2**d** and 2**f**) confirm comparable sizes with no noticeable aggregation. Given that ZSM-5 comprises micropores with a diameter of ~0.54 nm, size constraints limit the location of Pd NPs to within mesopores and on external surfaces only. This approach to spatial compartmentalisation has been previously demonstrated for both mesoporous-microporous zeolite and macroporous-mesoporous SBA-15 [19,21].

3.2. Characterisation of different micropore structure zeolite-based catalysts

The influence of the zeolite framework type (FAU, BEA and MFI), and hence intrinsic micropore sizes, zeolites USY (~0.74 nm), Beta (~0.67 nm), and ZSM-5 (~0.54 nm) [39] with comparable initial SAR values were used (Table S4). Fig. 3**a** displays the N_2 adsorption-desorption isotherms of the corresponding DPTA-treated zeolites, showing the presence of mesoporous features in all. HUSY-DA shows a higher mesopore surface area (228 m^2 g^{-1}), whereas HBETA-DA shows a significantly greater mesopore volume. The isotherm of HBETA-DA exhibits H4 hysteresis at a high relative pressure of $p/p_0 > 0.7$, consistent with inter-crystallite mesopores in between small crystallites [40]. Mesopore size distributions are presented in Fig. 3**b**, showing mesopores range from 4 to 32 nm for all three zeolites.

Zeolite acidity from NH_3-TPD (Fig. 3**c** and Table S5) reveals comparably strong acid site density (assessed at >350 °C) for HMZSM5-DA25 and HBETA-DA, whereas HUSY-DA possesses at least 25 % less. Moreover, variation in desorption temperature is also apparent, with HMZSM5-DA25 indicating to possess slightly stronger acid sites (higher desorption temperature) than the others. The variation may result from variations in bond angles of the T-O-T bond (T = tetrahedral atom, i.e., Si or Al) present in the different frameworks, i.e., 133°–177° for ZSM-5, 150° for BETA and 138°–147° for Y [41–43]. Analysis of the surface hydroxyls (acid sites) by DRIFTS is shown in Fig. 3**d**. The strong

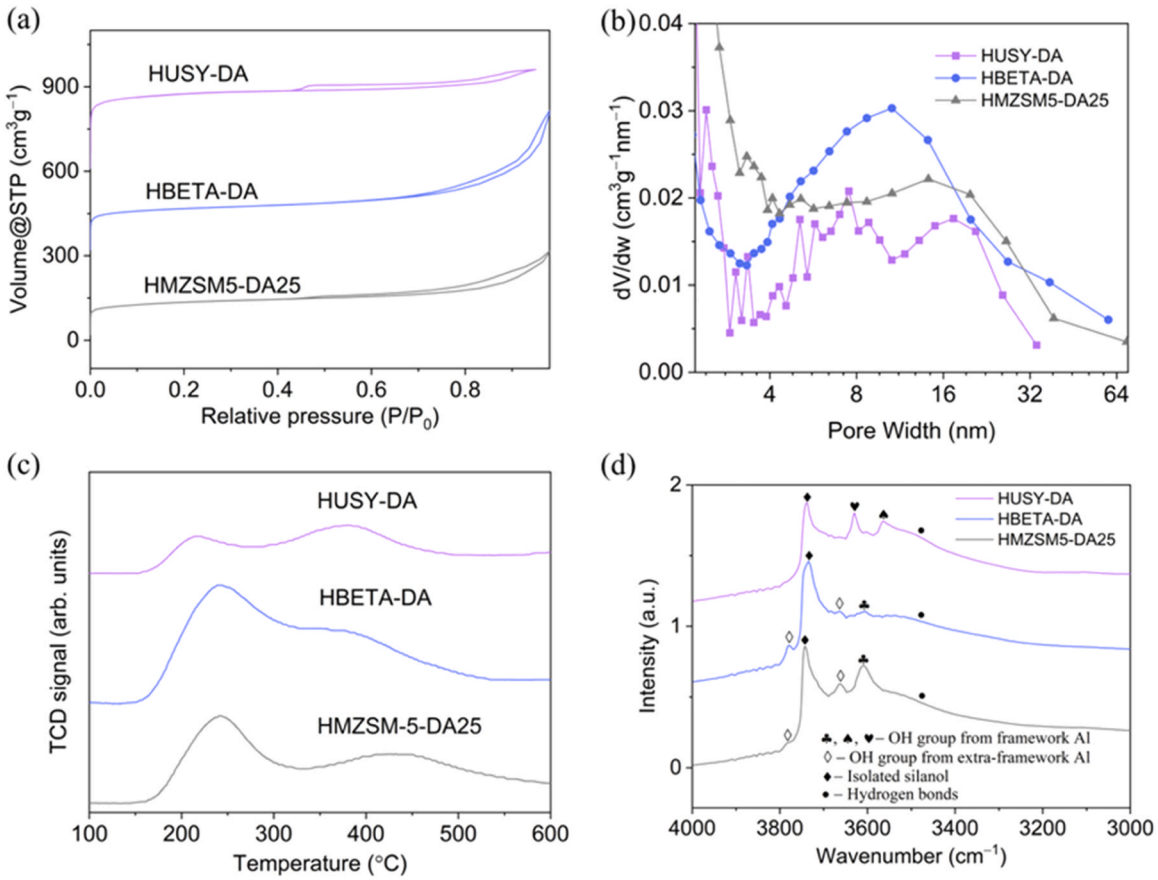

Fig. 3. Physicochemical properties of HUSY-DA, HBETA-DA and HMZSM5-DA25(a) N_2 adsorption-desorption isotherms, to aid visualisation, HBETA-DA and HUSY-DA are offset by 170 and 420 cm^3 g^{-1}, respectively; (b) Mesopore size distribution, in which dV/dw of HUSY-DA and H-MZSM5-DA25 are scaled by a factor of 3 and 1.5, respectively; (c) Mass normalised NH_3-TPD profiles; and (d) DRIFTS of OH region.

Brønsted acid site from Si(OH)Al for HBETA-DA and HMZSM5-DA25 present a peak at 3605 cm^{-1}, while for HUSY-DA, these species are observed at 3560 and 3628 cm^{-1}, reflecting whether located within the sodalite cage and the supercage, respectively [33,44,45]. Peaks at around 3660 cm^{-1} and 3780 cm^{-1} represent hydroxyl groups connected with extra-framework Al in all three zeolites. The peak at around 3745 cm^{-1} represents the isolated silanol groups of zeolites, while the shift to a lower wavenumber (3740–3730 cm^{-1}) suggests the existence of vicinal silanol groups (i.e., silanol nest). This is likely caused by dealumination, and the shift is due to the interaction of hydrogen bonds between vicinal silanol group, which can be observed as the broad peak at 3500–3200 cm^{-1} [46,47]. Silanol groups at 3742, 3738, and 3737 cm^{-1} were detected for HMZSM5-DA25, HBETA-DA and HUSY-DA, respectively, suggesting the presence of silanol nests. HUSY-DA and HBETA-DA have a higher degree of shift than HMZSM5-DA25, demonstrating that DPTA has a higher efficiency of dealumination over the zeolites with larger micropores.

Comparing and evaluating surface-probe interactions, from their

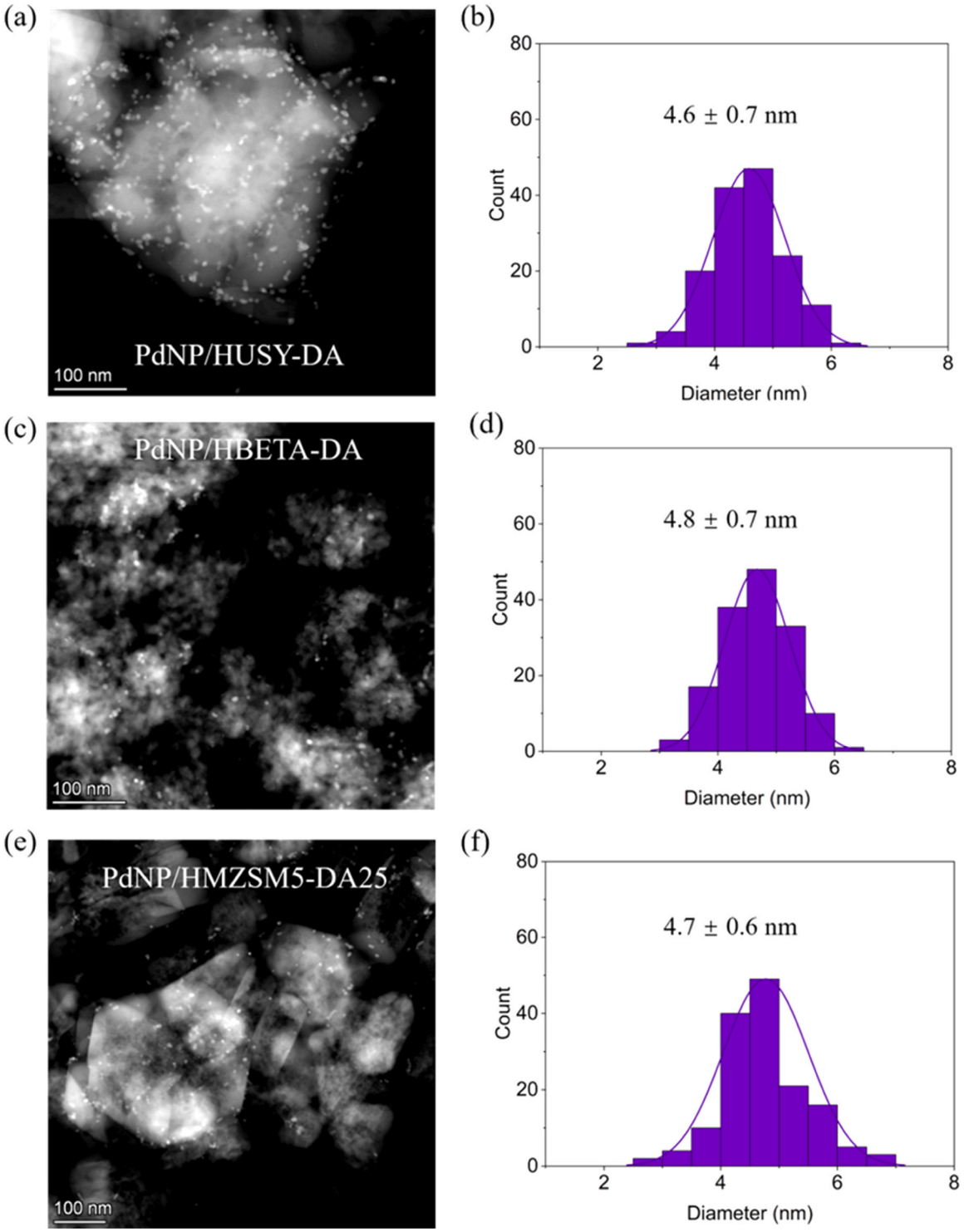

Fig. 4. Representative HAADF-STEM image of (a) PdNP/HUSY-DA; (b) PdNP/HBETA-DA; (c) PdNP/HMZSM5-DA25, (b), (d) and (f): the corresponding Pd particle size distributions.

respective T_1/T_2 values from NMR relaxation measurements, within a common zeolite framework is considered appropriate [48], given that any micropore confinement effects can be considered equal. In contrast, making comparable evaluations for a range of different frameworks is problematic as, in addition to surface interaction, molecule mobility can also be constrained, to varying degrees, by micropore confinement effects. This additional influence on T_1/T_2 values is indirectly proportional to micropore size, i.e. smaller pores result in a greater confinement effect, which in turn increases T_1/T_2 values. Thus, unravelling the origin of the higher T_1/T_2 *n*-octane value for the smaller pore HMZSM5-DA25 is not feasible, as the confinement effect would influence HMZSM5-DA25 more so than the other frameworks. Thus, the increased T_1/T_2 *n*-octane value for HMZSM5-DA25 could be due to either surface-probe interaction, micropore confinement, or a combination of both. It is, therefore, not possible to draw a conclusion regarding the oleophilicity of HUSY-DA, HBETA-DA and HMZSM5-DA25. However, in the case of water (kinetic diameter of 0.27 nm vs 0.48 nm for *n*-octane), any confinement effect across the three zeolite frameworks is overshadowed by a greater influence from the interaction between the surface and the probe (Table S6). While confinement will impact the smallest micropores of ZSM-5 the most, HMZSM5-DA25 exhibits the lowest T_1/T_2 value for water. Therefore, across these three zeolites T_1/T_2

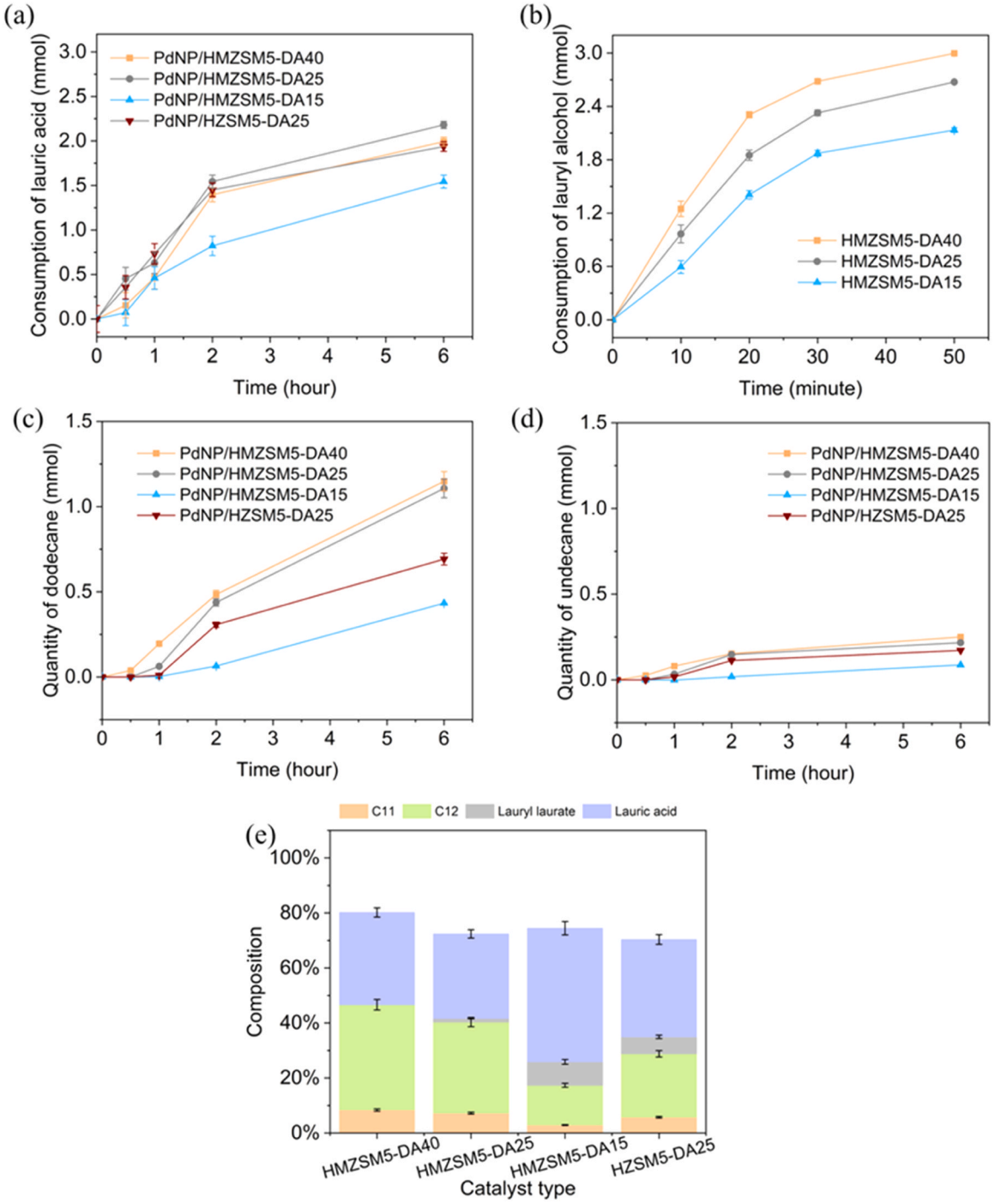

Fig. 5. Catalytic performance of 0.4 wt% PdNP/HMZSM5-DA40, PdNP/HMZSM5-DA25, PdNP/HMZSM5-DA15, PdNP/HZSM5-DA25. (a) lauric acid conversion via HDO of the fatty acid; (b) lauryl alcohol conversion (starting from the alcohol) over acid only equivalent catalysts, i.e. dehydration of the intermediate (note -dodecene was the only product detected; (c) dodecane yield from lauric acid HDO; (d) undecane yield from lauric acid HDO; (e) product distribution after 6 h.

values for water are dictated by interactions between the zeolite surface and water. Thus, HBETA-DA and HUSY-DA are more hydrophilic than HMZSM5-DA25.

The approach and subsequent results from the introduction of Pd NPs were consistent with the HMZSM5-DA series reported above. HAADF-STEM images of PdNP-doped HUSY-DA, HBETA-DA and HMZSM5-DA25 are presented in Fig. 4. Pd particle size distributions confirm uniform sizes across HUSY-DA, HBETA-DA and HMZSM5-DA25 (with particle diameters of around 4.7 nm) and no evidence of Pd agglomeration. In the case of PdNP/HBETA-DA, the micrographs reveal the smaller crystallites of the zeolite, which are attributed to giving rise to the greater degree of mesopore volume (N_2 adsorption isotherms) from inter-crystallite voids.

3.3. Catalytic performance for lauric acid HDO

The catalytic performance of the PdNP/HMZSM5-DA*x* series is shown in Fig. 5. With respect to lauric acid consumption (Fig. 5**a**), PdNP/HMZSM5-DA15 presents lower conversion than the other PdNP/HMZSM5-DA*x* catalysts. This could reflect its lower mesoporosity, i.e., a diffusion effect, or its greater total acidity and resultant hydrophilicity. To assess the impact of mesoporosity on the conversion of the starting substrate, a comparison of two comparable SAR species but with (PdNP/HMZSM5-DA25) and without (PdNP/HZSM5-DA25) significant mesoporous reveals this not to be the dictating parameter. Given the high Pd accessibility in both cases, the latter possessing all Pd sites on its external surface, this is not surprising. Thus, acidity, either directly or indirectly, is responsible for the reduced efficiency of PdNP/HMZSM5-DA15. Interaction between acidity and Pd has been shown to impact hydrodeoxygenation activity negatively [14]; however, this is less likely here, given the extraction of acid sites from all locations except micropores via the dealumination treatment. Thus, we tentatively ascribe stronger water affinity to be the cause, with increased water retention in the zeolite framework of PdNP/HMZSM5-DA15, hindering the initial acid reduction step for which water is the byproduct. Similar negative correlations between hydrophilicity and catalytic performance are also known for esterification reaction over ZSM-5 [49], and alcohol dehydration [50,51], both of which yield water as the byproduct. As observed here, decreasing SAR results in increased hydrophilicity, which hinders esterification through competitive adsorption of water at the catalytic site [49]. For the HDO cascade, the elevated localised water concentration within the zeolite framework either impacts the equilibrium of the fatty acid hydrogenation (first step) and/or negatively impacts the rate of the subsequent second step in the cascade, i.e., lauryl alcohol dehydration [50]. While lauryl alcohol is not detected in the liquid phase, lauryl laurate is (to be discussed below). The basis of the negative impact of water on alcohol dehydration could be diffusion, i.e., limiting diffusion of lauryl alcohol to the acid sites, or equilibrium, slowing the forward reaction of the alcohol dehydration step, or active site adsorption/transition state stabilisation. Either way, slowing the consumption of the intermediate alcohol will be unfavourable for fatty acid hydrodeoxygenation via equilibrium effects, i.e., its localised retention within the catalyst architecture framework slows the first step of the cascade while also prohibiting the cascade reaction from being driven to completion.

Fig. 5**b** illustrates the performance of the HMZSM5-DA*x* series for the dehydration of lauryl alcohol. Given that this step in the cascade is acid site catalysed, HMZSM5-DA15 could be anticipated to perform favourably. However, this is not the case. Brønsted acid could also be considered a key parameter, but this also does not appear to be the controlling factor, with no correlation between performance and Brønsted or Lewis acidity. Thus, it suggests mesoporosity is a key property. Increasing performance of the series directly correlates to mesoporosity, and while HMZSM5-DA15 shows greater hydrophilicity, which is expected to impart a negative effect, it is not the sole contributor as PdNP/HMZSM5-DA40 outperforms PdNP/HMZSM5-DA25 despite possessing an almost identical affinity to water. The benefit of mesoporosity is ascribed to improved diffusion, a common observation in catalysis employing hierarchical bimodal porous materials, which arises from greater accessibility of the smaller pores via the larger pores [52]. However, it is pointed out that in the case of the cascade, lauryl alcohol is formed within the mesopores, and thus, the beneficial role may be less within the cascade process.

As shown in Fig. 5**c**, the production of the desired C_{12} alkane (dodecane) is comparable over PdNP/HMZSM5-DA40 and PdNP/HMZSM5-DA25, ~1.1 mmol in 6 h. In contrast, PdNP/HMZSM5-DA15 yields a lower amount of dodecane at ~0.43 mmol. Having established the consequence of acidity and/or hydrophilicity on catalyst performance, part of this reduced performance can be attributed to this; however, it is also apparent that mesoporosity is a critical factor. This time, the comparison of PdNP/HMZSM5-DA25 and PdNP/HZSM5-DA25 demonstrates the latter is less capable of producing dodecane (i.e., 1.1 vs 0.69 mmol), confirming the beneficial impact of mesoporosity on the HDO cascade, i.e., diffusion of substrate and intermediates within the framework and the diffusion of the product out of the catalyst. Undecane represents the major byproduct of the process, with its production levels shown in Fig. 5**d**. It is generated by decarboxylation (of lauric acid) and/or decarbonylation (of lauraldehyde, an intermediate of lauric acid conversion) over Pd sites [2,53], and thus arises during the first step of the process. Across all PdNP/HMZSM5-DA*x* catalysts, a common C_{12}:C_{11} of ~5 is observed. Given this equal preference for HDO vs DCO_x, the environment of Pd sites within the mesopores and on the outer surface of the catalysts can be considered equivalent and is the only factor in dictating the degree of DCO_x observed. While the absolute level of DCO_x is lower for PdNP/HMZSM5-DA15, this solely reflects the lower lauric acid conversion. The compositions of the reactions after 6 h are shown in Fig. 5**e**. In addition to the products already discussed, the formation of lauryl laurate via esterification between the fatty acid and fatty alcohol is also observed for SAR $\leq$ 26. Increasing acidity drives this reaction, indicating at least partial conversion is zeolite catalysed by silanols on the surface of zeolite frameworks and acid sites within the micropore close to the pore entrance [54–56]. In addition, self-catalysis by unreacted lauric acid is also feasible, as indicated by the higher levels of lauryl laurate for PdNP/HZSM5-DA25 vs PdNP/HMZSM5-DA25. The latter is attributed to the less efficient diffusion of lauryl alcohol into the micropores (for dehydration), resulting in a greater amount diffusing back into the bulk solution. While the esterification is reversible, the preference is to avoid its formation in the first place to maximise cascade process efficiency.

Further expansion of this approach to HDO catalyst systems probed the role of zeolite framework, in which Pd nanoparticles were deposited on HUSY-DA, HBETA-DA and HMZSM5-DA25, all comprising comparable SAR, with catalyst performance reported in Fig. 6. Lauric acid conversion over PdNP/HBETA-DA and PdNP/HMZSM5-DA25, which possess similar micropore frameworks consisting of uniform channels, show similar rates of ~7.1 ± 0.7 mmol acid $g_{catalyst}^{-1}$ h^{-1} over the initial 2 h (Fig. 6**a**). However, their rates of dodecane formation do diverge, with the larger micropore PdNP/HBETA-DA showing a 17 % increase in production rate (Fig. 6**c**). Akin performance for fatty acid conversion reflects comparable Pd sites (Pd size) and Pd site accessibility (mesoporosity – surface area), and while HBETA-DA is more hydrophilic, this must be overcome by the larger micropore size and more facile diffusion of water out of the zeolite framework, which in turn benefits the overall cascade and, thus, dodecane formation. Further increasing micropore size, i.e., deploying PdNP/USY-DA, results in a further increase in catalytic performance, again overcoming amplified hydrophilicity and reduced acidity, with the larger micropore enhancing lauric acid conversion through superior fatty alcohol consumption (Fig. 6**b**), which reflects greater diffusion within the large micropores (pore aperture of 0.74 nm with a pore cavity of 1.3 nm, comparatively, MFI channel diameters are 0.54 nm). This reduced diffusion limitation is hinted at by the significantly reduced contribution (lower values) of confinement

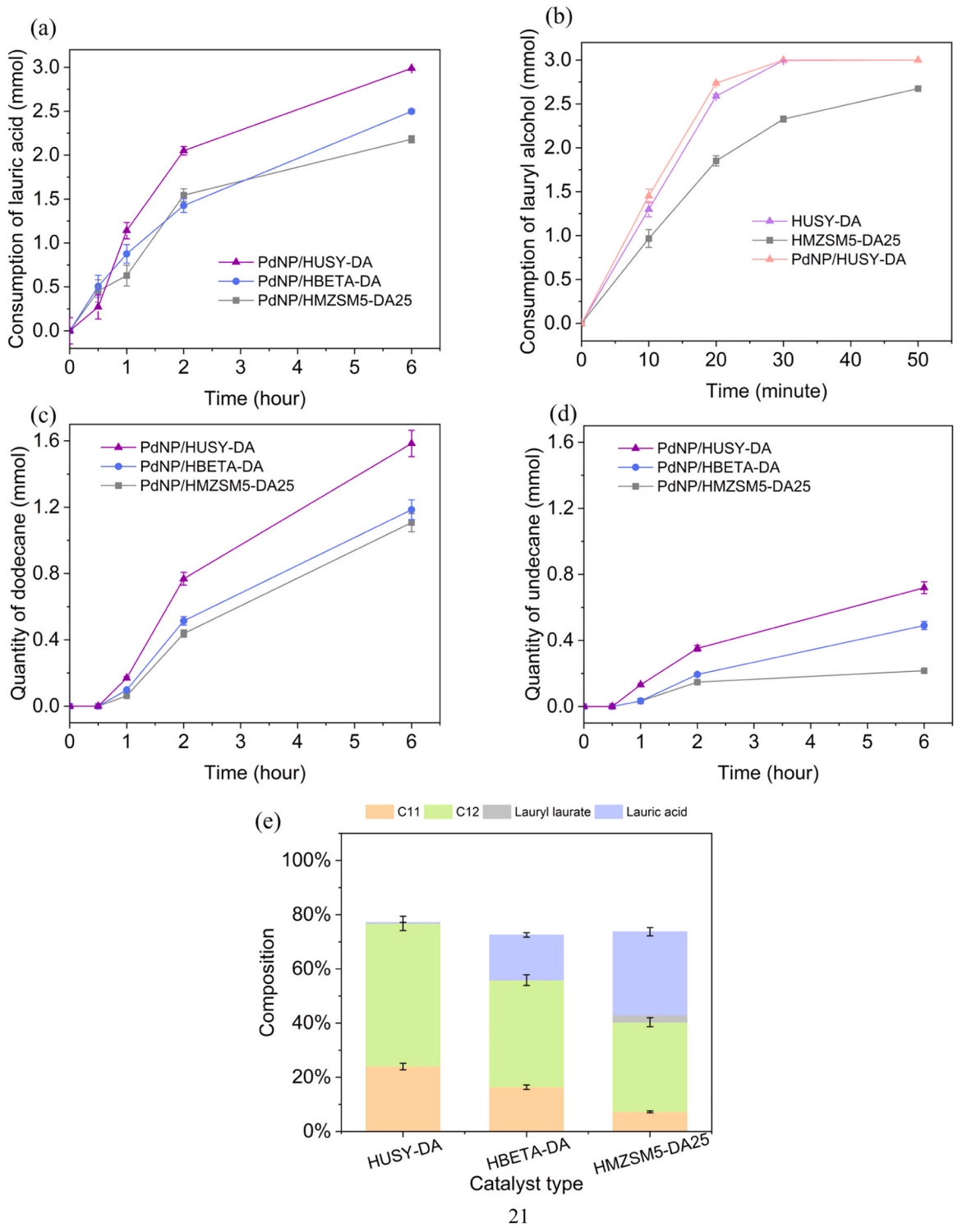

Fig. 6. Catalytic performance of PdNP/HUSY-DA, PdNP/HBeta-DA, PdNP/HMZSM5-DA25. (a) lauric acid conversion via HDO of the fatty acid; (b) lauryl alcohol conversion (starting from the alcohol) over acid only equivalent catalysts, i.e. dehydration of the intermediate (note - dodecene was the only product detected; (c) dodecane yield from lauric acid HDO; (d) undecane yield from lauric acid HDO; (e) product distribution after 6 h.

effects on the *n*-octane T_1/T_2 value for HUSY-DA (Table S6). Thus, mass transport rather than acidity dictated the second step of the HDO cascade, which in turn drives the chemical equilibrium of lauric acid conversion over Pd sites [57]. The dictating role of mass diffusion over acidity for the second step is further apparent from the superiority of HUSY-DA relative to the more acidic HMZSM5-DA25, as shown in Fig. 6**b**. Furthermore, the comparison of HUSY-DA to PdNP/HUSY-DA demonstrates that Pd does not facilitate alcohol conversion, ruling out alcohol reduction to dodecane over Pd sites under these reaction conditions (Pd-catalysed alcohol reduction to alkanes requires temperatures $>$ 300 °C) [58]. The overall outcome of the accumulation of these beneficial properties bestowed on PdNP/HUSY-DA is an optimal dodecane production rate of 6.1 $mmol_{dodecane}\ g_{catalyst}^{-1}\ h^{-1}$. However, the elevated performance of PdNP/HUSY-DA intensifies undecane yields, as

indicated in Fig. 6**d**. The increased conversion rates of lauric acid and dodecene, the intermediate from alcohol dehydration, result in more rapid consumption of surface H_2. This being critical to the desirable formation of surface Pd hydride, the reported active phase for HDO, whereas in the absence of surface Pd hydride, i.e., the presence of a metallic Pd surface, DCO_x becomes more prevalent [59]. The absence of the detection of lauryl laurate over PdNP/HUSY-DA (Fig. 6**e**) further reflects the greater internal diffusion and consumption of the lauryl alcohol intermediate.

The stability of the Pd sites of spent PdNP/HUSY-DA, PdNP/HBETA-DA, and PdNP/HMZSM5-DA25 is confirmed by HAADF-STEM, as shown in Fig. 7. Compared to the fresh catalysts (Fig. 4), the size of Pd NPs on the used counterpart is comparable (at <5 nm). Thus, this approach to catalyst design for cascade processes, via a strategy of spatial segregation of active sites, is a generic and effective way to stabilise Pd NPs on zeolitic carriers regardless of the type of framework.

Based on the findings reported here, and our previous publication [21], the advantages of the spatial compartmentalisation of two distinct active species, namely Pd NPs and acids site, within two different pore regions, these being mesopores and micropores, within a hierarchical porous material for HDO are illustrated in Fig. 8. The catalytic HDO cascade of lauric acid proceeds initially through its hydrogenation over

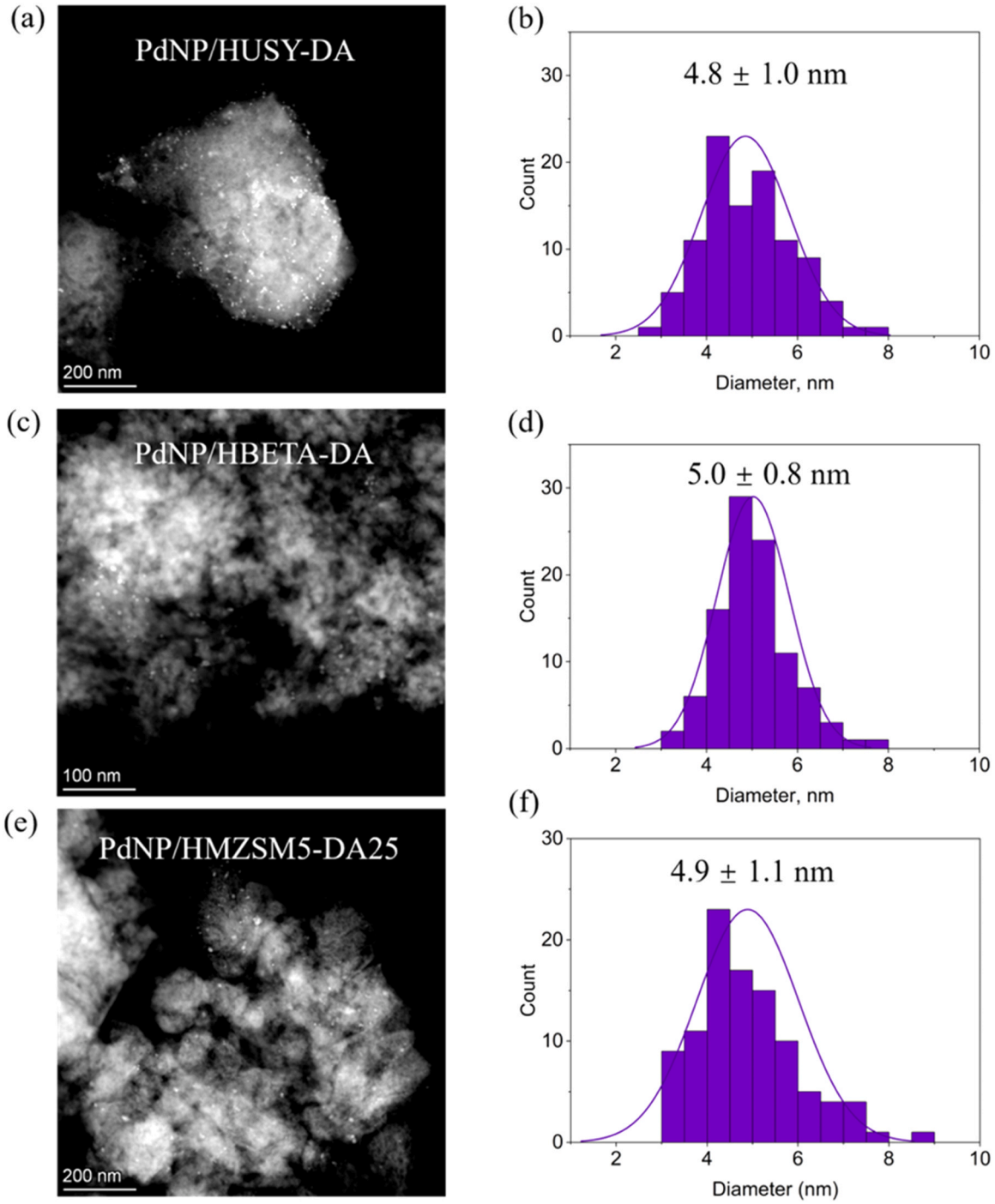

Fig. 7. Representative HAADF-STEM image of spent (a) PdNP/HMZSM5-DA, (b) PdNP/HBETA-DA, and (c) PdNP/HUSY-DA after the 6-h HDO reactions; (b), (d), (f): the corresponding particle size distribution for the used catalysts.

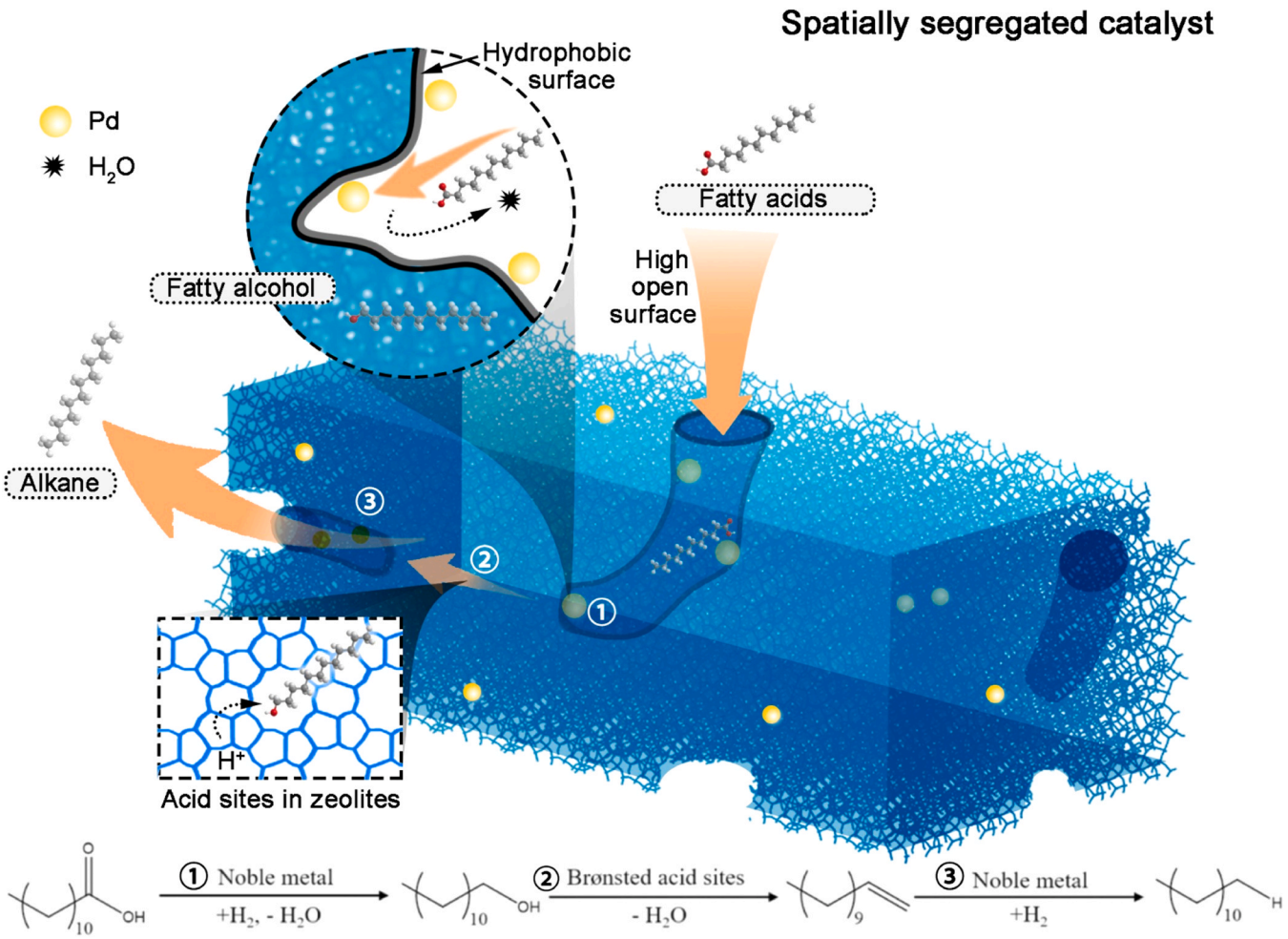

Fig. 8. Schematic diagram of spatially segregated catalysts for HDO of fatty acids to alkanes.

mesopore contained Pd NP sites, generating lauryl alcohol as an intermediate. Diffusion of this into the micropore network of the hierarchical zeolite framework facilitates its dehydration to dodecene (as identified by studies of acid catalysts alcohol dehydration in Figs. 5**b** and 6**b**) over acid sites, which reside solely in the micropores. Dodecene is subsequently rapidly hydrogenated into dodecane over the Pd site as it diffuses out of the porous catalyst. We attribute, at least partially, the benefit of these systems to result from control over the cascade process and their ability to drive the equilibrium of each step, through consumption of the intermediate products, which in turn drives reactant conversion. Inclusion of mesopores, as a site to host Pd NP, is beneficial to catalyst stability and in separating them from the acid site of the framework [21], promoting the first step of the cascade. Tuning the acidity of the micropore framework, through controlling the Si:Al, reveals that lower acid site density is preferable, potentially a result of the correlation of hydrophilicity with acidity. Reducing acidity thus minimises water (byproduct) retention within the micropore (retention of water slows the rate of substrate consumption, possibly also due to equilibrium effects). In contrast, increasing micropore size, through control of the zeolite framework deployed, has a positive impact which can be assigned to greater in-pore diffusion of reactants and products.

A comparison of our most active HDO systems with reported studies in which Pd is deployed as the active metal site is presented in Table S7, revealing preferential performance with respect to productivity and/or selectivity towards HDO, which is achieved by turning off DCO_x chemistry through the unique design of our catalytic system.

4. Conclusion

Built on the previous success of synthesising a new hydrodeoxygenation (HDO) catalyst using the spatial segregation strategy, this study elucidates the critical roles of acidity, mesoporosity, and micropore size in determining the catalytic HDO cascade performance of spatially segregated PdNP/zeolite catalysts in HDO of lauric acid (dodecane as the target product). Among the ZSM-5-based catalysts, hierarchical mesoporous structures enhance lauric acid conversion by 58 % compared to their microporous counterparts, primarily due to improved mass transport and reduced water retention. This was found to enhance the diffusion of intermediate lauryl alcohol, accelerating the overall activity of HDO (regarding the yield of dodecane) and suppressing the side-reaction (esterification). High acidity and hydrophilicity in ZSM-5 zeolites negatively affect HDO efficiency, hindering lauric acid conversion by retaining water within the framework, which adversely affects reaction equilibria in the HDO cascade, leading to a 61 % decrease in dodecane yield for the most acidic zeolite. Comparison of zeolitic frameworks reveals that PdNP/USY, with its larger micropores (~0.74 nm), achieves a dodecane production rate of 6.1 mmol $g_{catalyst}^{-1}$ h^{-1}, a 17 % improvement over PdNP/HBETA-DA and a 32 % enhancement over PdNP/HMZSM5-DA25, highlighting the advantage of the improved internal diffusion in the micropore regimes. Despite the enhanced performance, PdNP/HUSY-DA also exhibits the highest undecane selectivity, indicating increased decarboxylation/decarbonylation due to accelerated lauryl alcohol consumption. Catalyst stability assessments via HAADF-STEM confirm that Pd nanoparticles remain below 5 nm after prolonged reactions, ensuring catalyst durability.

These findings establish spatially segregated metal nanoparticle zeolite catalysts as an effective design approach for optimising HDO efficiency, reinforcing the necessity of fine-tuning porosity and acidity to maximise biofuel yield and minimise undesirable side reactions.

CRediT authorship contribution statement

Yani Peng: Writing – review & editing, Methodology, Investigation. **Carmine D'Agostino:** Writing – review & editing, Resources, Methodology, Investigation, Formal analysis. **Run Zou:** Writing – review & editing, Methodology, Investigation. **Ushna Khalid:** Writing – review & editing, Methodology, Investigation. **Min Hu:** Writing – review & editing, Methodology, Investigation, Formal analysis. **Shengzhe Ding:** Writing – original draft, Visualization, Methodology, Investigation, Formal analysis, Data curation, Conceptualization. **Xiaolei Fan:** Writing – review & editing, Supervision, Resources, Funding acquisition, Formal analysis, Conceptualization. **Parlett Christopher M. A.:** Writing – review & editing, Supervision, Methodology, Investigation, Formal analysis, Conceptualization. **Yilai Jiao:** Writing – review & editing, Resources, Methodology, Investigation. **Qiang Zhang:** Writing – review & editing, Methodology, Investigation.

Declaration of Competing Interest

The authors declare that they have no known competing financial interests or personal relationships that could have appeared to influence the work reported in this paper.

Acknowledgements

This project has received funding from the European Union's Horizon 2020 research and innovation programme under grant agreement No 872102. C.D. and X.F. would like to acknowledge the EPSRC (EP/V026089/1) for supporting their research activities. UK Catalysis Hub is kindly thanked for the resources and support provided via our membership of the UK Catalysis Hub Consortium and funding by EPSRC grant: EP/R026815/1 (C.M.A.P). This Project is also supported by the National Natural Science Foundation of China (No. 22378407 and W2431016) for research and collaboration. M.H. and R.Z. thank the financial support from the China Scholarship Council (file no. 201806340224 and 201906740020) and The University of Manchester (United Kingdom) for supporting their PhD research at The University of Manchester.

Appendix A. Supporting information

Supplementary data associated with this article can be found in the online version at doi:10.1016/j.mtcata.2025.100129.

References

[1] R.A. Sheldon, Biocatalysis and biomass conversion: enabling a circular economy, Philos. Trans. R. Soc. A Philos. T R. Soc. A 378 (2176) (2020) 2–19, https://doi.org/10.1098/rsta.2019.0274.
[2] S. Ding, C.M.A. Parlett, X. Fan, Recent developments in multifunctional catalysts for fatty acid hydrodeoxygenation as a route towards biofuels, Mol. Catal. 523 (2022).
[3] S. Khan, A.N.K. Lup, K.M. Qureshi, F. Abnisa, W.M.A.W. Daud, M.F.A. Patah, A review on deoxygenation of triglycerides for jet fuel range hydrocarbons, J. Anal. Appl. Pyrolysis 140 (2019) 1–24.
[4] D. Singh, K.A. Subramanian, M.O. Garg, Comprehensive review of combustion, performance and emissions characteristics of a compression ignition engine fueled with hydroprocessed renewable diesel, Renew. Sust. Energ. Rev. 81 (2018) 2947–2954, https://doi.org/10.1016/j.rser.2017.06.104.
[5] M.C. Chiong, C.T. Chong, J.-H. Ng, S.S. Lam, M.-V. Tran, W.W.F. Chong, M. N. Mohd Jaafar, A. Valera-Medina, Liquid biofuels production and emissions performance in gas turbines: a review, Energy Convers. Manag 173 (2018) 640–658, https://doi.org/10.1016/j.enconman.2018.07.082.
[6] A. O'Connell, M. Kousoulidou, L. Lonza, W. Weindorf, Considerations on GHG emissions and energy balances of promising aviation biofuel pathways, Renew. Sust. Energ. Rev. 101 (2019) 504–515, https://doi.org/10.1016/j.rser.2018.11.033.
[7] M. Ameen, M.T. Azizan, S. Yusup, A. Ramli, M. Yasir, Catalytic hydrodeoxygenation of triglycerides: an approach to clean diesel fuel production, Renew. Sust. Energ. Rev. 80 (2017) 1072–1088, https://doi.org/10.1016/j.rser.2017.05.268.
[8] H. Liu, J. Han, Q. Huang, H. Shen, L. Lei, Z. Huang, Z. Zhang, Z.K. Zhao, F. Wang, Catalytic hydrodeoxygenation of methyl stearate and microbial lipids to diesel-range alkanes over Pd/HPA-SiO2 catalysts, Ind. Eng. Chem. Res. 59 (39) (2020) 17440–17450, https://doi.org/10.1021/acs.iecr.0c02187.
[9] C. Perego, R. Millini, Porous materials in catalysis: challenges for mesoporous materials, Chem. Soc. Rev. 42 (9) (2013) 3956–3976.
[10] Q. Sun, N. Wang, J. Yu, Advances in catalytic applications of zeolite-supported metal catalysts, Adv. Mater. 33 (51) (2021) e2104442, https://doi.org/10.1002/adma.202104442.
[11] X. Cao, J. Zhao, F. Long, X. Zhang, J. Xu, J. Jiang, Al-modified Pd@mSiO2 core-shell catalysts for the selective hydrodeoxygenation of fatty acid esters: influence of catalyst structure and Al atoms incorporation, Appl. Catal. B Environ. 305 (2022), https://doi.org/10.1016/j.apcatb.2022.121068.
[12] M. Shahinuzzaman, Z. Yaakob, Y. Ahmed, Non-sulphide zeolite catalyst for bio-jet-fuel conversion, Renew. Sustain. Energy Rev. 77 (2017) 1375–1384, https://doi.org/10.1016/j.rser.2017.01.162.
[13] Y. Shi, Y. Cao, Y. Duan, H. Chen, Y. Chen, M. Yang, Y. Wu, Upgrading of palmitic acid to iso-alkanes over bi-functional Mo/ZSM-22 catalysts, Green. Chem. 18 (17) (2016) 4633–4648, https://doi.org/10.1039/c6gc01367h.
[14] M. Arroyo, L. Briones, H. Hernando, J.M. Escola, D.P. Serrano, selective decarboxylation of fatty acids catalyzed by Pd-supported hierarchical ZSM-5 zeolite (Article.), Energy Fuels 35 (21) (2021) 17167–17181, https://doi.org/10.1021/acs.energyfuels.1c01373.
[15] C. Gao, J. Zhang, E. Xing, Y. Xie, H. Zhao, P. Ning, Y. Shi, Upgrading of palmitic acid to diesel-like fuels over Ni@HZSM-5 bi-functional catalysts through the in situ encapsulation method, Mol. Catal. 511 (2021), https://doi.org/10.1016/j.mcat.2021.111715.
[16] Y. Shi, E. Xing, K. Wu, J. Wang, M. Yang, Y. Wu, Recent progress on upgrading of bio-oil to hydrocarbons over metal/zeolite bifunctional catalysts, Catal. Sci. Technol. 7 (12) (2017) 2385–2415, https://doi.org/10.1039/c7cy00574a.
[17] Z. Guo, F. Zhou, H. Wang, X. Liu, G. Xu, Y. Zhang, Y. Fu, Highly selective conversion of natural oil to alcohols or alkanes over a Pd stabilized CuZnAl catalyst under mild conditions, Green. Chem. 21 (18) (2019) 5046–5052, https://doi.org/10.1039/c9gc02379h.
[18] J. Zecevic, G. Vanbutsele, K.P. de Jong, J.A. Martens, Nanoscale intimacy in bifunctional catalysts for selective conversion of hydrocarbons, Nature 528 (7581) (2015) 245–248, https://doi.org/10.1038/nature16173.
[19] Christopher M.A. Parlett, Mark A. Isaacs, Simon K. Beaumont, Laura M. Bingham, Nicole S. Hondow, K. Wilson, Adam F. Lee, Spatially orthogonal chemical functionalization of a hierarchical pore network for catalytic cascade reactions, Nat. Mater. 15 (2) (2016) 178–182, https://doi.org/10.1038/nmat4478.
[20] M.A. Isaacs, C.M.A. Parlett, N. Robinson, L.J. Durndell, J.C. Manayil, S. K. Beaumont, S. Jiang, N.S. Hondow, A.C. Lamb, D. Jampaiah, et al., A spatially orthogonal hierarchically porous acid–base catalyst for cascade and antagonistic reactions, Nat. Catal. 3 (11) (2020) 921–931, https://doi.org/10.1038/s41929-020-00526-5.
[21] S. Ding, D.L. Fernandez Ainaga, M. Hu, B. Qiu, U. Khalid, C. D'Agostino, X. Ou, B. Spencer, X. Zhong, Y. Peng, et al., Spatial segregation of catalytic sites within Pd doped H-ZSM-5 for fatty acid hydrodeoxygenation to alkanes, Nat. Commun. 15 (1) (2024) 7718, https://doi.org/10.1038/s41467-024-51925-2 (From NLM PubMed-not-MEDLINE).
[22] J.C. Groen, L.A.A. Peffer, J.A. Moulijn, Perez-Ramirez, J. On the introduction of intracrystalline mesoporosity in zeolites upon desilication in alkaline medium (Article.), Microporous Mesoporous Mat. 69 (1-2) (2004) 29–34, https://doi.org/10.1016/j.micromeso.2004.01.002.
[23] S. Abdulridha, R. Zhang, S. Xu, A. Tedstone, X. Ou, J. Gong, B. Mao, M. Frogley, C. Bawn, Z. Zhou, et al., An efficient microwave-assisted chelation (MWAC) post-synthetic modification method to produce hierarchical Y zeolites, Microporous Mesoporous Mat. 311 (2021), https://doi.org/10.1016/j.micromeso.2020.110715.
[24] Y. Wang, A. Biby, Z. Xi, B. Liu, Q. Rao, X. Xia, One-pot synthesis of single-crystal palladium nanoparticles with controllable sizes for applications in catalysis and biomedicine, ACS Appl. Nano Mater. 2 (7) (2019) 4605–4612, https://doi.org/10.1021/acsanm.9b00963.
[25] J.C. Groen, Pérez-Ramírez, J. Critical appraisal of mesopore characterization by adsorption analysis, Appl. Catal. A Gen. 268 (1) (2004) 121–125, https://doi.org/10.1016/j.apcata.2004.03.031.
[26] E. Fukushima, Experimental pulse NMR: a nuts and bolts approach, CRC Press, 2018.
[27] H.Y. Carr, E.M. Purcell, Effects of diffusion on free precession in nuclear magnetic resonance experiments, Phys. Rev. 94 (3) (1954) 630.
[28] S.-J. Liaw, T.-L. Tso, Standardizing GC-FID measurement of nonmethane hydrocarbons in air for international intercomparison using retention index and effective carbon number concept, J. Anal. Sci. Technol. 8 (4) (1995) 807–814.
[29] X. Ou, S. Xu, J.M. Warnett, S.M. Holmes, A. Zaheer, A.A. Garforth, M.A. Williams, Y. Jiao, X. Fan, Creating hierarchies promptly: microwave-accelerated synthesis of ZSM-5 zeolites on macrocellular silicon carbide (SiC) foams, Chem. Eng. J. 312 (2017) 1–9.
[30] S.J. Gregg, K.S.W. Sing, H. Salzberg, Adsorption surface area and porosity, J. Electrochem. Soc. 114 (11) (1967) 279Ca.

[31] Y. Jiao, L. Forster, S. Xu, H. Chen, J. Han, X. Liu, Y. Zhou, J. Liu, J. Zhang, J. Yu, et al., Creation of Al-enriched mesoporous ZSM-5 nanoboxes with high catalytic activity: converting tetrahedral extra-framework Al into framework sites via post treatment, Angew. Chem. Int. Ed. 59 (2020) 19478–19486, https://doi.org/10.1002/anie.202002416.
[32] J.C. Groen, J.A. Moulijn, J. Pérez-Ramírez, Desilication: on the controlled generation of mesoporosity in MFI zeolites, J. Mater. Chem. 16 (22) (2006) 2121–2131.
[33] F.C. Meunier, D. Verboekend, J.-P. Gilson, J.C. Groen, J. Pérez-Ramírez, Influence of crystal size and probe molecule on diffusion in hierarchical ZSM-5 zeolites prepared by desilication, Microporous Mesoporous Mat. 148 (1) (2012) 115–121, https://doi.org/10.1016/j.micromeso.2011.08.002.
[34] N.-Y. Topsøe, K. Pedersen, E.G. Derouane, Infrared and temperature-programmed desorption study of the acidic properties of ZSM-5-type zeolites, J. Catal. 70 (1) (1981) 41–52.
[35] N. Robinson, P. Bräuer, A.P.E. York, C. D'Agostino, Nuclear spin relaxation as a probe of zeolite acidity: a combined NMR and TPD investigation of pyridine in HZSM-5, 10.1039/D1CP01515J, Phys. Chem. Chem. Phys. 23 (33) (2021) 17752–17760, https://doi.org/10.1039/D1CP01515J.
[36] K. Ralphs, C. D'Agostino, R. Burch, S. Chansai, L.F. Gladden, C. Hardacre, S. L. James, J. Mitchell, S.F.R. Taylor, Assessing the surface modifications following the mechanochemical preparation of a Ag/Al2O3 selective catalytic reduction catalyst, Catal. Sci. Technol. 4 (2) (2014) 531–539, https://doi.org/10.1039/c3cy00945a.
[37] C. D'Agostino, M.R. Feaviour, G.L. Brett, J. Mitchell, A.P.E. York, G.J. Hutchings, M.D. Mantle, L.F. Gladden, Solvent inhibition in the liquid-phase catalytic oxidation of 1,4-butanediol: understanding the catalyst behaviour from NMR relaxation time measurements, Catal. Sci. Technol. 6 (21) (2016) 7896–7901, https://doi.org/10.1039/c6cy01458e.
[38] S. Ballauri, E. Sartoretti, M. Hu, C. D'Agostino, Z. Ge, L. Wu, C. Novara, F. Giorgis, M. Piumetti, D. Fino, Praseodymium doping in ceria-supported palladium nanocatalysts as an effective strategy to minimize the inhibiting effects of water during methane oxidation, Appl. Catal. B Environ. 320 (2023) 121898.
[39] J. Cejka, A. Corma, S. Zones, Zeolites and catalysis: synthesis, reactions and applications, John Wiley & Sons, 2010.
[40] D.V. Peron, V.L. Zholobenko, M.R. de la Rocha, M. Oberson de Souza, L.A. Feris, N. R. Marcilio, V.V. Ordomsky, A.Y. Khodakov, Nickel–zeolite composite catalysts with metal nanoparticles selectively encapsulated in the zeolite micropores, J. Mater. Sci. 54 (7) (2019) 5399–5411.
[41] W. Aslam, M.M. Hossain, M.A. Bari Siddiqui, B.A. Abussaud, S.S. Al-Khattaf, Kinetics of liquid phase alkylation of benzene with dodecene over mordenite, Can. J. Chem. Eng. 93 (5) (2015) 870–880.
[42] J.A. van Bokhoven, D. Koningsberger, P. Kunkeler, H. Van Bekkum, A. Kentgens, Stepwise dealumination of zeolite βeta at specific T-sites observed with 27Al MAS and 27Al MQ MAS NMR, J. Am. Chem. Soc. 122 (51) (2000) 12842–12847.
[43] M. Boronat, A. Corma, Factors controlling the acidity of zeolites, Catal. Lett. 145 (2015) 162–172.
[44] C.J. Van Oers, K. Góra-Marek, K. Sadowska, M. Mertens, V. Meynen, J. Datka, P. Cool, In situ IR spectroscopic study to reveal the impact of the synthesis conditions of zeolite β nanoparticles on the acidic properties of the resulting zeolite, Chem. Eng. J. 237 (2014) 372–379, https://doi.org/10.1016/j.cej.2013.10.041.
[45] F. Lónyi, J. Valyon, G. Pál-Borbély, A DRIFT spectroscopic study of the N2 adsorption and acidity of H-faujasites, Microporous Mesoporous Mat. 66 (2-3) (2003) 273–282, https://doi.org/10.1016/j.micromeso.2003.09.018.
[46] F. Yi, Y. Chen, Z. Tao, C. Hu, X. Yi, A. Zheng, X. Wen, Y. Yun, Y. Yang, Y. Li, Origin of weak Lewis acids on silanol nests in dealuminated zeolite Beta, J. Catal. 380 (2019) 204–214, https://doi.org/10.1016/j.jcat.2019.10.008.
[47] I.C. Medeiros-Costa, E. Dib, N. Nesterenko, J.P. Dath, J.P. Gilson, S. Mintova, Silanol defect engineering and healing in zeolites: opportunities to fine-tune their properties and performances, Chem. Soc. Rev. 50 (19) (2021) 11156–11179, https://doi.org/10.1039/d1cs00395j (From NLM PubMed-not-MEDLINE).
[48] C. D'Agostino, A.P. York, P. Bräuer, Host-guest interactions and confinement effects in HZSM-5 and chabazite zeolites studied by low-field NMR spin relaxation, Mater. Today Chem. 24 (2022) 100901.
[49] E.G. Fawaz, D.A. Salam, T.J. Daou, Esterification of linoleic acid using HZSM-5 zeolites with different Si/Al ratios, Microporous Mesoporous Mater. 294 (2020) 109855, https://doi.org/10.1016/j.micromeso.2019.109855.
[50] Y. Zhi, H. Shi, L. Mu, Y. Liu, D. Mei, D.M. Camaioni, J.A. Lercher, Dehydration pathways of 1-propanol on HZSM-5 in the presence and absence of water, J. Am. Chem. Soc. 137 (50) (2015) 15781–15794, https://doi.org/10.1021/jacs.5b09107.
[51] M. He, M. Wang, G. Tang, Y. Fang, T. Tan, From medium chain fatty alcohol to jet fuel: Rational integration of selective dehydration and hydro-processing, Appl. Catal. A Gen. 550 (2018) 160–167, https://doi.org/10.1016/j.apcata.2017.11.009.
[52] C.M.A. Parlett, K. Wilson, A.F. Lee, Hierarchical porous materials: catalytic applications, 10.1039/C2CS35378D, Chem. Soc. Rev. 42 (9) (2013) 3876–3893, https://doi.org/10.1039/C2CS35378D.
[53] H.G. Manyar, C. Paun, R. Pilus, D.W. Rooney, J.M. Thompson, C. Hardacre, Highly selective and efficient hydrogenation of carboxylic acids to alcohols using titania supported Pt catalysts, Chem. Commun. 46 (34) (2010) 6279–6281.
[54] G. Mitran, S. Chen, K.L. Dolge, W. Huang, D.-K. Seo, Ketonic decarboxylation and esterification of propionic acid over beta zeolites, Microporous Mesoporous Mat. 310 (2021), https://doi.org/10.1016/j.micromeso.2020.110628.
[55] Y. Ye, M. Yao, H. Chen, X. Zhang, Influence of silanol defects of ZSM-5 zeolites on trioxane synthesis from formaldehyde, Catal. Lett. 150 (5) (2019) 1445–1453, https://doi.org/10.1007/s10562-019-03040-x.
[56] A. Brito, M. Borges, N. Otero, Zeolite Y as a heterogeneous catalyst in biodiesel fuel production from used vegetable oil, Energy Fuels 21 (6) (2007) 3280–3283.
[57] K.J. Laidler, Chemical Kinetics, Harper & Row, 1987.
[58] N. Chen, N. Wang, Y. Ren, H. Tominaga, E.W. Qian, Effect of surface modification with silica on the structure and activity of Pt/ZSM-22@SiO2 catalysts in hydrodeoxygenation of methyl palmitate, J. Catal. 345 (2017) 124–134, https://doi.org/10.1016/j.jcat.2016.09.005.
[59] L. Karam, C.N. Neumann, Heterogeneously catalyzed carboxylic acid hydrogenation to alcohols, ChemCatChem 14 (22) (2022), https://doi.org/10.1002/cctc.202200953.